

# Enhancing Perovskite Solar Cell Performance through Femtosecond Laser Polishing

Wenchi Kong, Chen Zhao, Jun Xing, Yuting Zou, Tao Huang, Feng Li, Jianjun Yang, Weili Yu,\* and Chunlei Guo\*

**Nonradiative recombination loss is a key process that determines the performance of perovskite solar cells, and how to control it is significant for the research and development of perovskites. Generally, traditional chemical modification/passivation methods are complicated and prone to secondary contamination. Herein, femtosecond (fs) laser polishing as a promising technique is demonstrated to ameliorate the surface of perovskite films, reduce nonradiative recombination loss, and improve solar cell performance. The high-intensity fs laser pulses can remove around 20 nm-thick perovskite top layer through an ionization process, help to decrease the grain boundary density, and enlarge the grain size of perovskite films after recrystallization. It is believed that fs laser polishing is a time-effective and highly precise technique that is suitable for large-scale device production, thus will trigger more applications in optoelectronics.**

In the past decade, the growing demands for renewable energy have pushed forward the research of high-efficiency solar cells utilizing halide perovskites as light absorber. Perovskite materials, which usually process the common formula of  $ABX_3$  ( $A = MA, FA, Cs$ , etc.;  $B = Pb, Sn$ , etc.;  $X = Cl, Br$ , or  $I$ ), have shown excellent physical properties and technological advantages, including tunable wavelength absorption, long carrier

diffusion length, long carrier lifetime, and easy for fabrication via spin coating or roll-to-roll techniques. It is reported that the power conversion efficiency (PCE) of perovskite solar cells has been keeping on increasing and the highest PCE over 25% have been achieved so far.<sup>[1–6]</sup> Currently, one key challenge for further enhancing the device performance is how to effectively minimize nonradiative recombination loss caused by the grains and grain boundaries that widely exist in the polycrystalline films.<sup>[7]</sup> To resolve this issue, much effort has been made following chemical modification/passivation strategies, e.g., solution-processed secondary growth (SSG) technique,<sup>[8]</sup> contact-passivation method,<sup>[2]</sup> and so on. However,

these reported methods are generally complicated and prone to secondary contamination. Novel techniques that can reduce the nonradiative recombination loss with high speed, high precision, and low contamination are thus desirable.

More recently, some groups have considered utilizing continuous laser to synthesize and treat the perovskite films for solar cell applications.<sup>[9–11]</sup> For example, Kim's group applied continuous near-infrared (NIR) laser processing for the perovskite films and achieved a reliable crystallization method for the perovskite solar cells.<sup>[9]</sup> In the meanwhile, Zou's group demonstrated NIR laser irradiation as an effective approach for the rapid crystallization of  $CH_3NH_3PbI_3$  films.<sup>[10]</sup> In addition, Yan's group tried to use continuous lasers with different wavelengths to treat the active films and achieved the high-efficiency solar cells.<sup>[11]</sup> Among these works, the continuous lasers were mainly utilized to help crystal formation due to their unique photothermal effect. In stark contrast, pulse lasers, especially high-energy pulse lasers, can normally make severe mechanical damage and are more suitable for ablation or cutting. Recently, Cheng's group reported that nanosecond laser processing can be a feasible method to release residual stress and a simple manner to improve the performance of perovskite electronics and optoelectronics.<sup>[12]</sup> However, for ultrafast pulsed laser, e.g., femtosecond (fs) laser, which has much higher energy than the nanosecond laser, few explorations were reported so far. Exploring the interaction between fs laser and perovskite is of significance for fundamental research, and how to apply it in optoelectronics is still an open question.<sup>[13–16]</sup>

Notably, it is critical to understand how the high-energy power pulse laser works during the processing before proposing a suitable method to utilize it. Laser as a powerful tool has been


W. Kong, C. Zhao, J. Xing, Y. Zou, T. Huang, Prof. J. Yang, Prof. W. Yu, Prof. C. Guo

The Guo Photonics Laboratory  
State Key Laboratory of Applied Optics  
Changchun Institute of Optics, Fine Mechanics and Physics  
Chinese Academy of Sciences  
Changchun 130033, P. R. China  
E-mail: weili.yu@ciomp.ac.cn; chunlei.guo@rochester.edu

W. Kong, C. Zhao, J. Xing, Y. Zou, T. Huang  
Department of Materials Science and Optoelectronics Engineering  
University of Chinese Academy of Sciences  
Beijing 100049, P. R. China

Prof. F. Li  
School of Physics  
Faculty of Science  
University of Sydney  
Sydney, NSW 2006, Australia

Prof. C. Guo  
The Institute of Optics  
University of Rochester  
Rochester, NY 14627, USA

 The ORCID identification number(s) for the author(s) of this article can be found under <https://doi.org/10.1002/solr.202000189>.

DOI: 10.1002/solr.202000189

applying in a quick growing number of civil and military fields, which can assist in achieving deposition, sintering, cutting, patterning, crystallization, scribing, and drilling with high degrees of precision and automation.<sup>[9,10,17–26]</sup> During laser processing, based on the knowledge of local interaction between laser radiation and the materials, the laser beam energy will be absorbed more or less, gradually causes local heating, melting, and even ablation.<sup>[27]</sup> In particular, the time duration of the pulsed laser plays a crucial role in determining the physical properties and subsequent macroscopic effects. Especially, when the pulse duration is tens of femtoseconds, the ultrafast fs laser would permit a so-called cold interaction with the matter,<sup>[17]</sup> avoiding the heat accumulation and the correlated unwanted secondary effects. The ultrashort duration of a fs pulse ( $\approx 10^{-15}$ – $10^{-14}$  s) is much shorter than the electron-lattice energy relaxation time and will thus cause a significant nonequilibrium state between electrons and lattices, resulting in a quick ionization process of the materials.<sup>[28,29]</sup> Ultrafast pulsed lasers thus allow for the processing such as cutting, drilling, carving, and patterning.<sup>[18]</sup> Beyond the aforementioned functions of laser processing techniques, laser polishing, that takes advantage of the laser energy to remove the undesirable components from a broad range of materials, is thus also attractive.<sup>[30]</sup>

Herein, we demonstrate that fs laser polishing can be an effective technique to optimize the surface morphology of perovskite polycrystalline films and reduce the possibility of nonradiative recombination happening, thus eventually improving the solar energy conversion performance. This work will trigger the application of fs laser as a powerful tool for perovskite materials

processing in not only solar cells but also light-emitting diodes (LEDs) and other optoelectronic applications.

We prepared the  $\text{Cs}_{0.06}\text{FA}_{0.79}\text{MA}_{0.15}\text{Pb}(\text{I}_{0.85}\text{Br}_{0.15})_3$  perovskite films using spin-coating method and tried to utilize fs laser processing to remove the protruding components that may cause nonradiative recombination. **Figure 1** shows the scheme of perovskite solar cell fabrication, in which two routes were applied to evaluate the effect of fs laser polishing. For route I (a–b–f–g–h), the solar cells were fabricated without laser processing (named as unprocessed in the figures). For route II (a–b–c–d–e–f–g–h), the fs laser processing was adapted to be a key step to ameliorate the perovskite layer surface morphology (named as processed in the figures). Photograph of the fs laser polishing system and optical image of laser-polished perovskite film are shown in Figure S1, Supporting Information, from which one can see the color of polished perovskite film areas gets darkened. After the fs laser polishing, rinsing by isopropanol and re-spin-coating  $\text{Cs}_{0.012}\text{MA}_{0.158}\text{FA}_{0.03}(\text{I}_{0.17}\text{Br}_{0.03})_3$  solution were applied, followed by annealing treatment to make sure that the surface of perovskite film was recrystallized.

The polishing functions of fs laser treatment process are achieved through the ionization of perovskite materials. The laser processing is reported to be related to three temporal parameters.<sup>[27]</sup> As normally defined,  $\tau_e$  is the electron cooling time, which is about 1 ps;  $\tau_l$  is lattice heating time, which is about 1 ns; and  $\tau_p$  is the time duration of laser pulse. Once  $\tau_l \ll \tau_e \ll \tau_l$  and pulse duration is within a few fs, electrons will absorb the laser pulse energy and transfer energy to ions rather than the lattice. In this case, the time duration of laser pulse is 35 fs,

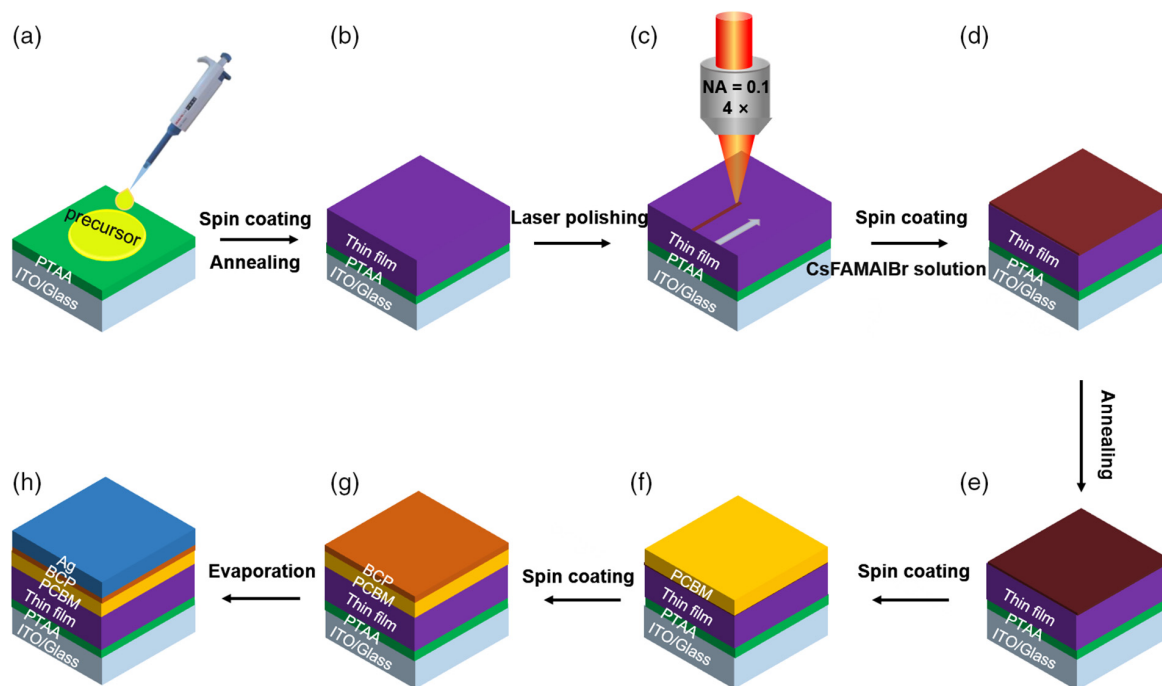


**Figure 1.** The scheme of perovskite solar cell fabrication processing with fs laser polishing as a key step to improve the perovskite layer surface morphology. a) Precursor solution was spread onto PTAA coated glass/ITO substrate. b) Perovskite thin film was formed by spin-coating and annealing. c) Perovskite thin film was exposed to femtosecond laser beam scan. d) As-deposited film was obtained by spin-coating  $\text{Cs}_{0.012}\text{MA}_{0.158}\text{FA}_{0.03}(\text{I}_{0.17}\text{Br}_{0.03})_3$  solution. e) The perovskite film was recrystallized. f) The electron transport layer PCBM was formed by spin-coating. g) BCP layer was obtained by spin-coating. h) The Ag electrode was deposited by thermal evaporation.

which is much shorter than the electron–lattice temperature equilibration time ( $10^{-10}$ – $10^{-12}$  s). And when the power intensity of fs laser goes up to  $10^{14}$  W cm $^{-2}$ , which is high enough to break the bonds of their molecular structure, it would excite the atoms into ions immediately. The pulse duration of 35 fs can thus lead to the precise removal of surface layers without any collateral damage to the underlying perovskite. Such process is so fast that the left atoms have no time to transfer energy to neighboring lattice, and thus there is no any melting produced on the perovskite surface.

The surface morphologies of perovskite film before and after fs laser processing are shown in **Figure 2**. The scanning electron microscopy (SEM) image of perovskite film before fs laser polishing in Figure 2a shows that the film is composed of grains with a wide size distribution from tens of nanometer to several hundred nanometers. After the fs laser polishing, as shown in Figure 2b, some tiny and bright crystals appear. According to the X-ray diffraction (XRD) test results shown in Figure S2a, Supporting Information, it can be concluded that they are PbI $_2$ . The formation of bright PbI $_2$  crystals can be attributed to the loss of carbon-containing component during the fs polishing.<sup>[8]</sup> From the energy dispersive spectrometry (EDS) spectra of perovskite before and after laser polishing, as shown in Figure S3 and S4, Supporting Information, the increased amount of PbI $_2$  is also observed, and the large grains lie beneath. The tiny PbI $_2$  crystals are produced because the fs pulse energy is much higher than the bond dissociation energy of the hybrid materials, which can cause the serious damage to some common organic/inorganic compounds,<sup>[31]</sup> and also the triple-cation-based perovskites like Cs $_{0.012}$ MA $_{0.158}$ FA $_{0.03}$ (I $_{0.17}$ Br $_{0.03}$ ) $_3$  here.<sup>[9,32]</sup> After fs laser processing, excessive PbI $_2$  as the impurities may induce nonradiative recombination and reduce the photoluminescence (PL) lifetime according to the time-resolved photoluminescence (TRPL) results

in Figure S2b, Supporting Information. Noted that the defocusing distance ( $D$ ) is a key parameter as well as scanning speed; when  $D$  is 600  $\mu$ m ( $1.26 \times 10^{12}$  W cm $^{-2}$  peak laser intensity), the laser polished perovskite film shows the best solar conversion efficiency, which will be discussed in the following parts.

After further spin-coating Cs $_{0.012}$ MA $_{0.158}$ FA $_{0.03}$ (I $_{0.17}$ Br $_{0.03}$ ) $_3$  solution and annealing, the SEM of perovskite film is shown in Figure 2c. Some of the bright PbI $_2$  crystals are washed away, and others react with Cs $_{0.012}$ MA $_{0.158}$ FA $_{0.03}$ (I $_{0.17}$ Br $_{0.03}$ ) $_3$  solution to regenerate perovskite polycrystal film and the grain size increase simultaneously. The EDS spectra of unprocessed and processed perovskite film are shown in Figure S3 and S5, Supporting Information, which indicate that the missing carbon-containing component has been restored. As the grain boundaries are the main place where nonradiative recombination may happen,<sup>[7]</sup> the decreasing amount of them and the enlarged grain size will benefit the charge transfer and collection. Figure 2d–f shows the cross-sectional morphologies of perovskite films corresponding to Figure 2a–c samples, respectively. It can be found that around 20 nm thickness of perovskite layer was removed by ionization process using fs laser. Before fs laser polishing, the perovskite film shows a rough surface with more grains, as shown in Figure 2d. After laser polishing and recrystallization, the perovskite film displays a smooth surface morphology with less grains, as shown in Figure 2f. The polishing effect can be further confirmed by the Keyence 3D laser microscopy measurements, as shown in Figure S6, Supporting Information. It is clearly shown that the surface of fs laser-processed sample becomes more uniform compared with the unprocessed one. The unprocessed samples show a  $R_a$  (arithmetical mean deviation) roughness of 42 nm, which is decreased to 22 nm after fs laser polishing, as shown in **Table 1**. The low roughness of perovskite active layer would

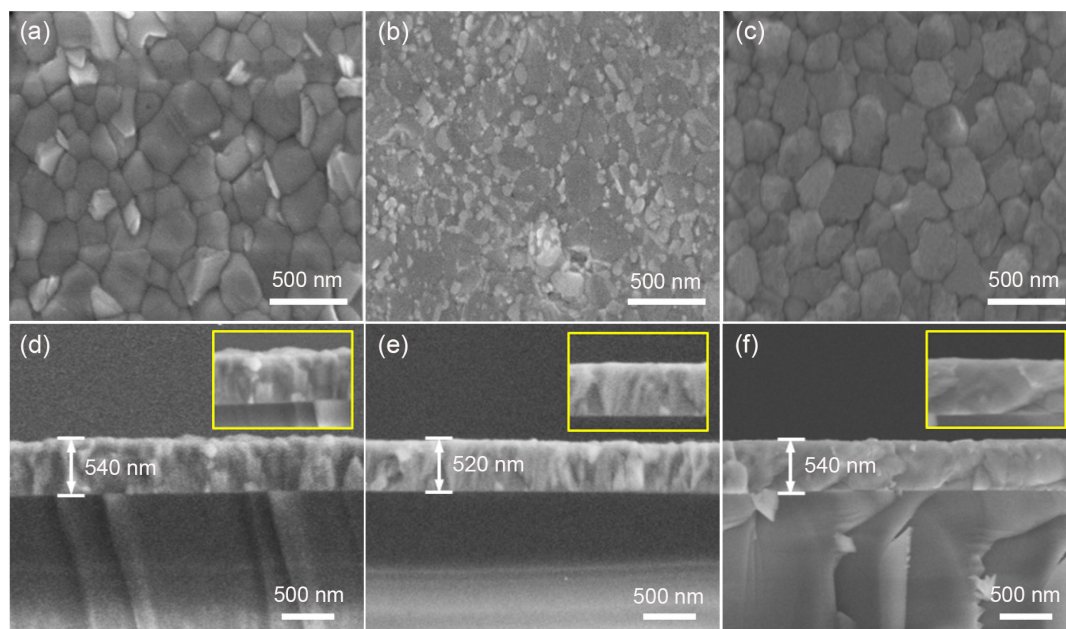


**Figure 2.** The surface morphologies of perovskite thin films of laser unprocessed, polished, and processed. The SEM images of a) fs laser unprocessed, b) polished, and c) processed perovskite film. d–f) The cross-sectional morphologies of perovskite films corresponding to (a)–(c) samples, respectively.

**Table 1.** The surface roughness  $R_a$  (arithmetical mean deviation) and  $R_q$  (root mean squared) in Figure S6, Supporting Information.

Region	$R_a$ [ $\mu\text{m}$ ]	$R_q$ [ $\mu\text{m}$ ]
Unprocessed	0.042	0.792
Processed	0.022	0.319

be favorable to the charge transfer with less risk of leakage happened.<sup>[33–37]</sup>

The properties of perovskite films before and after fs laser processing were further characterized by XRD and optical measurement methods. **Figure 3a** shows the XRD spectra of both perovskite films, which indicate that they both are  $\alpha$ -phase structured and the crystal structures can keep well after the fs laser processing.<sup>[8]</sup> The absorption spectra of both samples are shown in **Figure 3b** without apparent changing, indicating the absorption property of perovskite film is well maintained after laser processing. It also proves that the fs laser processing has no significant impact on the crystal structure and the corresponding band structure.<sup>[38]</sup> The effect of fs laser polishing on recombination properties of the perovskite films was then studied, aiming to clarify the defect state and recombination process within perovskite films.<sup>[7,39]</sup> The steady-state PL spectra of both samples are shown in **Figure 3c**. After fs laser processing, the PL intensity was greatly improved, revealing that defects were reduced and

the surface nonradiative recombination in the perovskite layer was inhibited.<sup>[40,41]</sup> We then performed TRPL measurements for both samples, and the results are shown in **Figure 3d**. The carrier recombination dynamics is represented by  $-\frac{dn}{dt} = C_1n + C_2n^2 + C_3n^3$ ,<sup>[42,43]</sup> where  $n$  is the photoexcited carriers density,  $t$  is the time, and the terms  $C_i n^i$  ( $i = 1, 2, 3$ ) represent defect trapping recombination (Shockley–Read–Hall recombination), free electron–hole recombination, and Auger recombination, respectively. Using a triexponential fitting for the processed and unprocessed films, the obtained results show that the processed films have a longer lifetime calculated as 44 ns (**Table 2**), indicating the lower nonradiative recombination due to a significant decrease in the concentration of defects and an increase in perovskite crystallinity.<sup>[3,44,45]</sup> In general, the improvement of PL intensity and the slow decay of PL lifetime obtained from the fs laser processed-perovskite film can be attributed to the reduction of trap recombination centers and grain boundaries. This is consistent with the aforementioned SEM results. The finding also shows a good agreement with previous reports that perovskite bulk crystals has a much larger carrier lifetime than polycrystals.<sup>[46,47]</sup>

Perovskite solar cells were then fabricated to examine the effect of fs laser polishing. Solar cells fabricated following Route I and II were both tested, and the current–voltage curves are shown in **Figure 4a**. For the fs laser-processed sample (Route II), the short-circuit current density ( $J_{sc}$ ) is  $23.31 \text{ mA cm}^{-2}$ , which is slightly higher than the value of  $23 \text{ mA cm}^{-2}$  for the

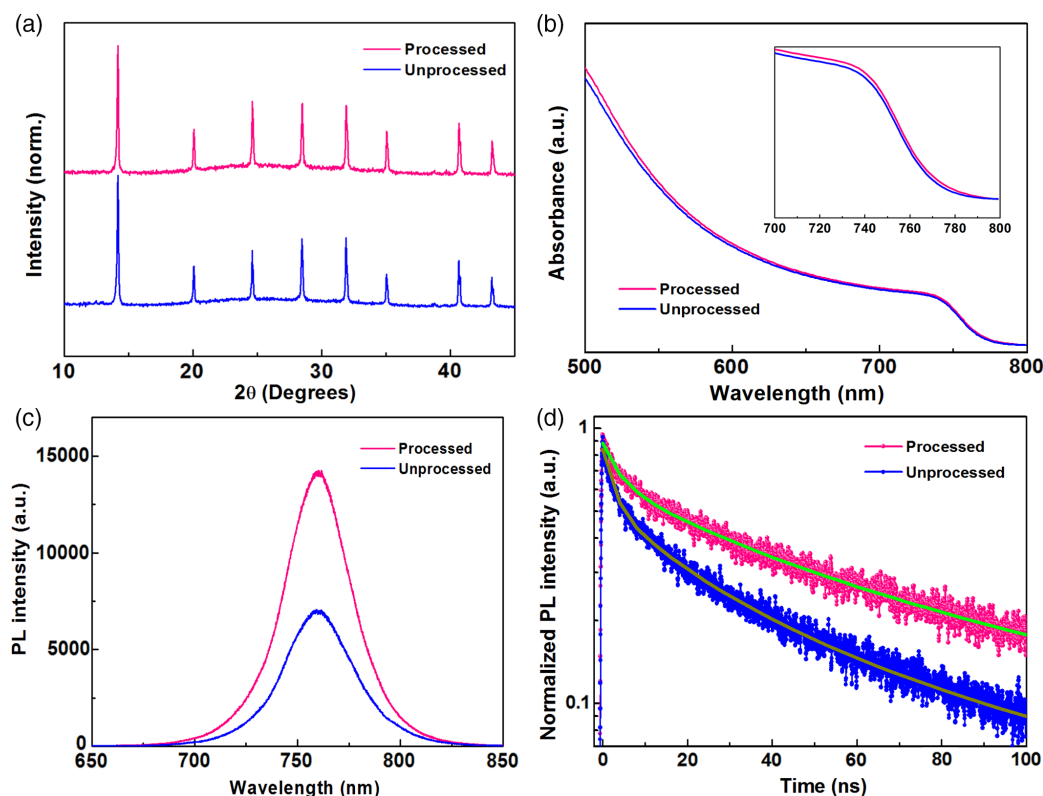


**Figure 3.** a) The XRD spectra of perovskite films both processed and unprocessed by fs laser. b) The absorption spectra of perovskite films both processed and unprocessed by fs laser. c) The steady-state photoluminescence spectra for processed and unprocessed perovskite films by fs laser. d) The TRPL spectra for processed and unprocessed perovskite films by fs laser.



**Table 2.** The PL lifetime obtained from processed and unprocessed region in Figure 3d.

Region	$\tau_1$ [ns]	$f_1$ [%]	$\tau_2$ [ns]	$f_2$ [%]	$\tau_3$ [ns]	$f_3$ [%]	$\tau_{\text{aver}}$ [ns]
Processed	2.5	2.2	22.4	13	108	84.8	44
Unprocessed	1.7	6.1	15.4	18.4	80.6	75.5	18

unprocessed sample, indicating the light absorption and excitons generation are not affected greatly. The  $J_{\text{sc}}$  was further confirmed by calculating the external quantum efficiency (EQE) in Figure 4b. The open-circuit voltage ( $V_{\text{oc}}$ ) increased from 1.08 to 1.14 V, which leads to a marked improvement of filled factor (FF) from 68.5% to 70.2%, due to shunt resistance increasing from 5182 to 41467  $\Omega$ . As a result, the PCE of solar cells increased from 17% (unprocessed) to 18.6% (processed). Noted that the improvement should be the synergistic effect of laser polishing and recrystallization rather than just a cleaning or recrystallization effect. To prove this, we further compared the unprocessed samples with the one that was treated by cleaning and recrystallization. In Figure S7, Supporting Information, it can be observed that both fluorescence intensity and life decrease slightly for the samples after cleaning and crystallization, indicating that cleaning and crystallization without fs laser polishing could even lead to increased defects. This further confirms that fs laser polishing is a key part. We also

performed the PL and TRPL measurements for the polycrystalline films processed under different defocusing conditions, and the results shown in Figure S8, Supporting Information, indicate both PL intensity and carrier lifetime enhanced comparing with the unprocessed ones.  $J$ - $V$  curves under different defocus conditions are shown in Figure S9, Supporting Information. The findings indicate that both PL and current density are closely linked to the defocusing distance during the polishing processing, which might be attributed to the spatial distribution of laser pulse energy.<sup>[48]</sup> The effect of defocus distance on device PCE was also examined, as shown in Figure 4c, which indicates that laser polishing is very sensitive to defocus distance. The stability test results for the solar cells are shown in Figure 4d, which imply that the laser-processed samples can maintain 84% PCE compared with that of the unprocessed samples that is 81% after 30 days. Overall, the aforementioned results indicate that fs laser polished samples have large shunt resistance that contributes to the enhanced FF, PCE, and stability.

In conclusion, we demonstrate that fs laser polishing is an effective technique to ameliorate the surface of perovskite films and reduce their nonradiative recombination loss, which can be utilized for improving the light-to-electric conversion efficiency. The fs laser can remove the protruding component by ultrafast ionization process, thus providing a novel passivation strategy for high-performance optoelectronic devices. This research extends the applications of pulsed laser from manufacturing processes

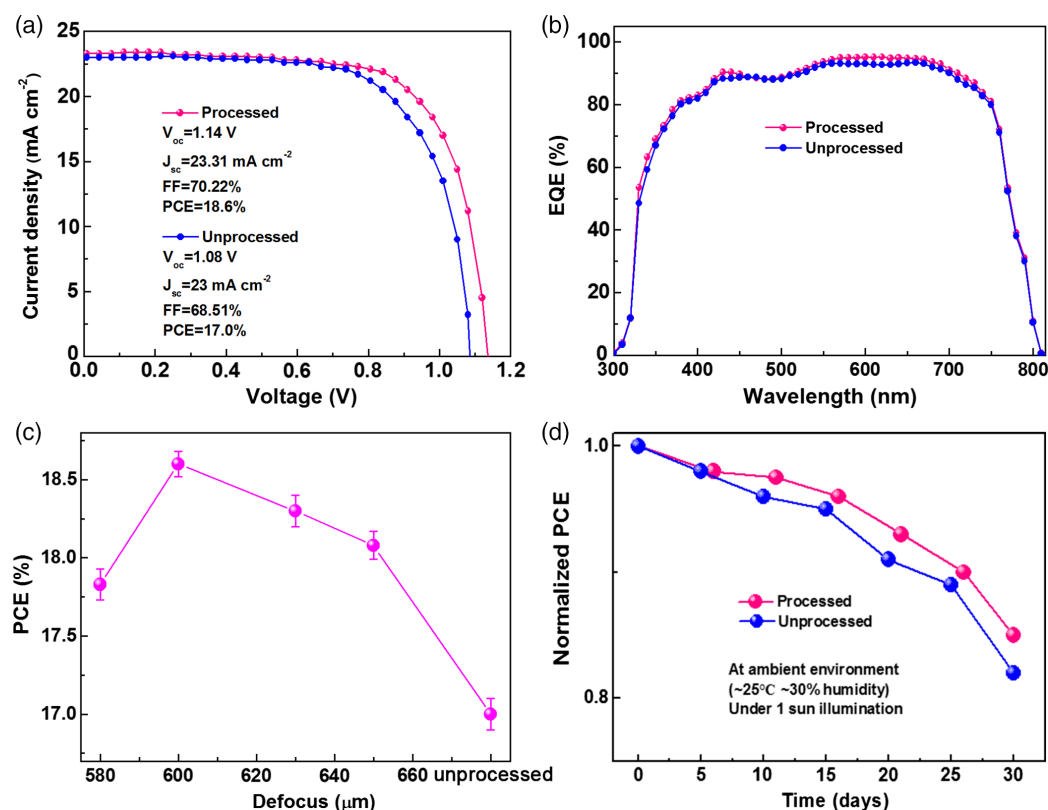


**Figure 4.** a) The  $J$ - $V$  spectra of solar cells based on both processed and fs laser unprocessed perovskite films. b) The EQE spectra of solar cells based on both processed and fs laser unprocessed perovskite films. c) The dependence of PCE on the defocus length during fs laser processing. d) The stability of solar cells based on both fs laser processed and unprocessed perovskite films.

(like cutting, drilling, scribing, etc.) to active layer treatment processing, makes a further step for pulsed layer application in the photovoltaic field. We believe this work will trigger more research on such processing strategy in the solar cells, LEDs, or imaging fields.

## Experimental Section

**Materials:** Methylamine solution (40% aqueous solution), formamidine acetate (99%), and lead bromide ( $\text{PbBr}_2$ , 99%) were all purchased from Aladdin Company. Lead iodide ( $\text{PbI}_2$ ,  $\geq 99.99\%$ ), formamidine iodide (FAI), methylammonium bromide (MABr), cesium iodide (CsI,  $\geq 99.99\%$ ), poly[bis(4-phenyl)(2,4,6-trimethylphenyl)amine] (PTAA), and [6,6]-phenyl-C<sub>61</sub>-butyric acid methyl ester (PCBM) ( $>99\%$ , Nichem Fine Technology Co., Ltd.) were all bought from Xi'an Polymer Light Technology Corp. *N,N*-Dimethylformamide (DMF, 99.8%), dimethyl sulfoxide (DMSO,  $\geq 99.9\%$ ), chlorobenzene (CB, 99.8%), and isopropanol (IPA, 99.5%) were all got from Sigma-Aldrich.

**Synthesis FAI and MABr:** FAI was synthesized according to the previously reported method.<sup>[47,49]</sup> First, formamidine acetate (52 g) was added into hydroiodic acid solution (80 mL) in ice water mixture for 6 h with stirring. Second, the solution was evaporated in the rotary evaporation at 60 °C for 3 h to obtain white powder. Third, the white powder was washed in anhydrous ethanol and recrystallized in anhydrous ether for 3 times. Finally, the FAI was collected by filtration and placed in a vacuum drying oven for 12 h.

MABr was synthesized according to the previously reported method.<sup>[47,49]</sup> First, 44 mL HBr acid solution and 30 mL methylamine solution were mixed at 0 °C for 2 h with stirring. Then the solvent was removed to obtain the white powder by rotary evaporation at 60 °C. Next, the white powder (MABr) was redissolved in anhydrous ethanol and recrystallized with anhydrous ether for 3 times. Finally, the MABr was collected by filtration and dried at 60 °C in a vacuum for one night.

**Solar Cell Fabrication and fs Laser Polishing:**  $\text{F}_4\text{-TCNQ}$  in CB ( $1 \text{ mg mL}^{-1}$ ) was stirred at 60 °C for 12 h.  $\text{F}_4\text{-TCNQ}$  was added into PTAA solution ( $6 \text{ mg mL}^{-1}$  in CB) with a weight ratio of 1%, and then the PTAA-coated ITO substrates were heated at 120 °C for 15 min. To improve the wettability of perovskite precursor on the PTAA, 100  $\mu\text{L}$  DMF was spin-coated at a speed of 5000 rpm for 10 s prior to perovskite films deposition. The triple-cation-based perovskite  $\text{Cs}_{0.06}\text{FA}_{0.79}\text{MA}_{0.15}\text{Pb}(\text{I}_{0.85}\text{Br}_{0.15})_3$  was prepared by dissolving  $\text{PbI}_2$  (1.2 M),  $\text{PbBr}_2$  (0.21 M), MABr (0.21 M), and FAI (1.11 M) in a mixture of DMF:DMSO (4:1 volume ratio, v:v) followed by addition of 5 vol% CsI stock solution (1.5 M in DMSO). A two-step process is used to spin coat the perovskite solution at 2000 and 6000 rpm for 15 and 35 s, respectively, adding 190  $\mu\text{L}$  drop of chlorobenzene 35 s after the start of the spinning routine. The samples were immediately annealed on a hotplate at 100 °C for 1 h. After fs laser polishing perovskite film, the processed perovskite film was rinsed with isopropanol and spin-coated solution of MABr (0.042 M) and FAI (0.222 M) and CsI (0.03 M) in isopropanol (1 mL) at 4000 rpm for 30 s, and then put on a hotplate at 100 °C for 30 min. Conditions for fs laser processing of perovskite thin films: under the condition that scanning speed  $v = 0.4 \text{ mm s}^{-1}$ , defocus  $D = 600 \mu\text{m}$  ( $1.26 \times 10^{12} \text{ W cm}^{-2}$  peak laser intensity) is the optimal condition. The defocusing distances of  $D = 630 \mu\text{m}$  ( $1.14 \times 10^{12} \text{ W cm}^{-2}$ ),  $D = 650 \mu\text{m}$  ( $1.07 \times 10^{12} \text{ W cm}^{-2}$ ), and  $D = 580 \mu\text{m}$  ( $1.35 \times 10^{12} \text{ W cm}^{-2}$ ) were all conducted and the results were summarized. The PCBM solution in chlorobenzene (20  $\text{mg mL}^{-1}$ ) was then spin-coated on top of the perovskite layer at 3000 rpm for 30 s. The bathocuproin (BCP) solution in IPA (0.5  $\text{mg mL}^{-1}$ ) was spin-coated at 5000 rpm for 30 s. Finally, 100 nm Ag counter electrode was deposited by thermal evaporation. All the film preparations were performed in a nitrogen-filled glove box.

**Fs Laser System:** In the fs laser system, we used the linearly polarized 35 fs laser pulse trains at a repetition rate of 1 kHz with the central wavelength  $\lambda = 800 \text{ nm}$ , and the maximum average energy of  $\approx 7 \text{ mJ}$ , which is generated by a chirped-pulse amplification of Ti:sapphire laser system (Spitfire Ace, Spectra Physics).

**Characterizations and Measurements:** Morphology and cross section of perovskite film layer in the processed and unprocessed region were obtained from Hitachi S-4800. We used the BRUKER D8 focusing in room temperature air for XRD measurement. We used Agilent Cary 5000 to record the absorption spectra of perovskite film. We used HORIBA Scientific Raman Spectrometer to obtain PL spectra with 532 nm in air. We used MicroTime 200 Time-resolved Fluorescence Microscope (PicoQuant) to obtain TRPL spectra with 532 nm laser excitation at room temperature in air. We used the Phenom Element Identification application attached to the Phenom Pro-X to obtain energy-dispersive spectrometry (EDS) mapping of perovskite film. We used KEYENCE VK-X200 3D laser scanning microscope to measure 3D pseudocolor plots and the surface roughness ( $R_a$  and  $R_q$ ). The  $J$ - $V$  curves were obtained by using a Keithley 2400 Source Meter under simulated 1 sun AM1.5G illumination ( $100 \text{ mW cm}^{-2}$ ) with a solar simulator. The  $J$ - $V$  curves for all devices were measured in ambient air under 25 °C temperature and 30% humidity, and the samples were light soaked for 5 min before collecting data.

## Supporting Information

Supporting Information is available from the Wiley Online Library or from the author.

## Acknowledgements

This work was supported by the National Key Research and Development Program of China (grant nos. 2018YFB1107202 and 2017YFB1104700), the National Natural Science Foundation of China (NSFC 61774155, 91750205, and 61705227), the K. C. Wong Education Foundation (GJT-D-2018-08), and the Open Project of State Key Laboratory of Supramolecular Structure and Materials (SKLSSM202034).

## Conflict of Interest

The authors declare no conflict of interest.

## Keywords

femtosecond lasers, optoelectronics, perovskites, solar cells

Received: April 7, 2020

Revised: May 2, 2020

Published online: May 20, 2020

- [1] Q. Han, Y.-T. Hsieh, L. Meng, J.-L. Wu, P. Sun, E.-P. Yao, S.-Y. Chang, S.-H. Bae, T. Kato, V. Bermudez, Y. Yang, *Science* **2018**, 361, 904.
- [2] W. S. Yang, J. H. Noh, N. J. Jeon, Y. C. Kim, S. Ryu, J. Seo, S. I. Seok, *Science* **2015**, 348, 1234.
- [3] W. S. Yang, B.-W. Park, E. H. Jung, N. J. Jeon, Y. C. Kim, D. U. Lee, S. S. Shin, J. Seo, E. K. Kim, J. H. Noh, S. I. Seok, *Science* **2017**, 356, 1376.
- [4] H. Zhou, Q. Chen, G. Li, S. Luo, T.-B. Song, H.-S. Duan, Z. Hong, J. You, Y. Liu, Y. Yang, *Science* **2014**, 345, 542.
- [5] H. Tan, A. Jain, O. Voznyy, X. Lan, F. P. G. de Arquer, J. Z. Fan, R. Quintero-Bermudez, M. Yuan, B. Zhang, Y. Zhao, F. Fan, P. Li, L. N. Quan, Y. Zhao, Z.-H. Lu, Z. Yang, S. Hoogland, E. H. Sargent, *Science* **2017**, 355, 722.
- [6] National Renewable Energy Laboratory, Best research-cell efficiencies chart, <http://www.nrel.gov/pv/> (accessed: August 2019).

- [7] D. W. de Quilettes, S. M. Vorpahl, S. D. Stranks, H. Nagaoka, G. E. Eperon, M. E. Ziffer, H. J. Snaith, D. S. Ginger, *Science* **2015**, 348, 683.
- [8] D. Luo, W. Yang, Z. Wang, A. Sadhanala, Q. Hu, R. Su, R. Shivanna, G. F. Trindade, J. F. Watts, Z. Xu, T. Liu, K. Chen, F. Ye, P. Wu, L. Zhao, J. Wu, Y. Tu, Y. Zhang, X. Yang, W. Zhang, R. H. Friend, Q. Gong, H. J. Snaith, R. Zhu, *Science* **2018**, 360, 1442.
- [9] T. Jeon, H. M. Jin, S. H. Lee, J. M. Lee, H. I. Park, M. K. Kim, K. J. Lee, B. Shin, S. O. Kim, *ACS Nano* **2016**, 10, 7907.
- [10] F. Li, W. Zhu, C. Bao, T. Yu, Y. Wang, X. Zhou, Z. Zou, *Chem. Commun.* **2016**, 52, 5394.
- [11] P. You, G. Li, G. Tang, J. Cao, F. Yan, *Energy Environ. Sci.* **2020**, 13, 1187.
- [12] C. P. Song, L. Tong, F. Liu, L. Ye, G. J. Cheng, *Adv. Funct. Mater.* **2019**, 30, 1906781.
- [13] W. Y. Nie, H. H. Tsai, R. Asadpour, J. C. Blancon, A. J. Neukirch, G. Gupta, J. J. Crochet, M. Chhowalla, S. Tretiak, M. A. Alam, H. L. Wang, A. D. Mohite, *Science* **2015**, 347, 522.
- [14] J. S. Huang, Y. C. Shao, Q. F. Dong, *J. Phys. Chem. Lett.* **2015**, 6, 3218.
- [15] Z. G. Xiao, Y. B. Yuan, Y. C. Shao, Q. Wang, Q. F. Dong, C. Bi, P. Sharma, A. Gruverman, J. S. Huang, *Nat. Mater.* **2015**, 14, 193.
- [16] H. J. Yen, P. W. Liang, C. C. Chueh, Z. B. Yang, A. K. Y. Jen, H. L. Wang, *ACS Appl. Mater. Interfaces* **2016**, 8, 14513.
- [17] L. Jiang, A.-D. Wang, B. Li, T.-H. Cui, Y.-F. Lu, *Light: Sci. Appl.* **2018**, 7, 17134.
- [18] G. Mincuzzi, A. L. Palma, A. Di Carlo, T. M. Brown, *Chemelectrochem* **2016**, 3, 9.
- [19] J. R. de Abajo, B. E. Jorge, J. M. G. Martin, H. C. Diaz, J. F. L. Ferrer, A. A. Lopez, *Int. J. Ophthalmol.* **2019**, 12, 961.
- [20] Y. X. Tan, W. Chu, P. Wang, W. B. Li, J. Qi, J. Xu, Z. S. Wang, Y. Cheng, *Phys. Scr.* **2019**, 94, 015501.
- [21] E. O. Olakanmi, R. F. Cochrane, K. W. Dalgarno, *Prog. Mater. Sci.* **2015**, 74, 401.
- [22] S. Mishra, V. Yadava, *Opt. Laser Eng.* **2015**, 73, 89.
- [23] C. W. Visser, R. Pohl, C. Sun, G. W. Roemer, B. H. in 't Veld, D. Lohse, *Adv. Mater.* **2015**, 27, 4087.
- [24] S. E. Burns, K. Reynolds, W. Reeves, M. Banach, T. Brown, K. Chalmers, N. Cousins, M. Etchells, C. Hayton, K. Jacobs, A. Menon, S. Siddique, P. Too, C. Ramsdale, J. Watts, P. Cain, T. von Werne, J. Mills, C. Curling, H. Sirringhaus, K. Amundson, M. D. McCreary, *J. Soc. Inf. Display* **2005**, 13, 583.
- [25] S. R. Bakaul, W. Lin, T. Wu, *Appl. Phys. Lett.* **2012**, 100, 012403.
- [26] J. F. Ding, Z. P. Lin, J. C. Wu, Z. L. Dong, T. Wu, *Small* **2015**, 11, 576.
- [27] J. Mazumder, *J. Laser Appl.* **2001**, 13, 177.
- [28] K. Sugioka, Y. Cheng, *Light: Sci. Appl.* **2014**, 3, e149.
- [29] M. Malinauskas, A. Žukauskas, S. Hasegawa, Y. Hayasaki, V. Mizeikis, R. Buividas, S. Juodkazis, *Light: Sci. Appl.* **2016**, 5, e16133.
- [30] P. Ortiz, V. Antunez, R. Ortiz, J. M. Martin, M. A. Gomez, A. R. Hortal, B. Martinez-Haya, *Appl. Surf. Sci.* **2013**, 283, 193.
- [31] S. J. Blanksby, G. B. Ellison, *Acc. Chem. Res.* **2003**, 36, 255.
- [32] G. D. Niu, W. Z. Li, F. Q. Meng, L. D. Wang, H. P. Dong, Y. Qiu, *J. Mater. Chem. A* **2014**, 2, 705.
- [33] W. L. Yu, F. Li, H. Wang, E. Alarousu, Y. Chen, B. Lin, L. F. Wang, M. N. Hedhili, Y. Y. Li, K. W. Wu, X. B. Wang, O. F. Mohammed, T. Wu, *Nanoscale* **2016**, 8, 6173.
- [34] J. Meyer, S. Hamwi, M. Kroger, W. Kowalsky, T. Riedl, A. Kahn, *Adv. Mater.* **2012**, 24, 5408.
- [35] Y. X. Zhao, A. M. Nardes, K. Zhu, *Appl. Phys. Lett.* **2014**, 104, 213906.
- [36] P. Gao, M. Gratzel, M. K. Nazeeruddin, *Energy Environ. Sci.* **2014**, 7, 2448.
- [37] S. Kazim, M. K. Nazeeruddin, M. Gratzel, S. Ahmad, *Angew. Chem. Int. Ed.* **2014**, 53, 2812.
- [38] S. J. Kim, J. Byun, T. Jeon, H. M. Jin, H. R. Hong, S. O. Kim, *ACS Appl. Mater. Interfaces* **2018**, 10, 2490.
- [39] Q. S. Dong, Y. T. Shi, K. Wang, Y. Li, S. F. Wang, H. Zhang, Y. J. Xing, Y. Du, X. G. Bai, T. L. Ma, *J. Phys. Chem. C* **2015**, 119, 10212.
- [40] B. X. Chen, W. G. Li, H. S. Rao, Y. F. Xu, D. B. Kuang, C. Y. Su, *Nano Energy* **2017**, 34, 264.
- [41] Q. Jiang, Y. Zhao, X. W. Zhang, X. L. Yang, Y. Chen, Z. M. Chu, Q. F. Ye, X. X. Li, Z. G. Yin, J. B. You, *Nat. Photonics* **2019**, 13, 500.
- [42] J. S. Manser, P. V. Kamat, *Nat. Photonics* **2014**, 8, 737.
- [43] S. Chen, X. Wen, R. Sheng, S. Huang, X. Deng, M. A. Green, A. Ho-Baillie, *ACS Appl. Mater. Interfaces* **2016**, 8, 5351.
- [44] J. M. Bing, J. Kim, M. Zhang, J. H. Zheng, D. S. Lee, Y. Cho, X. F. Deng, C. F. J. Lau, Y. Li, M. A. Green, S. J. Huang, A. W. Y. Ho-Baillie, *Small* **2019**, 15, 1804858.
- [45] A. O. El-Ballouli, O. M. Bakr, O. F. Mohammed, *Chem. Mater.* **2019**, 31, 6387.
- [46] Q. Dong, Y. Fang, Y. Shao, P. Mulligan, J. Qiu, L. Cao, J. Huang, *Science* **2015**, 347, 967.
- [47] D. Shi, V. Adinolfi, R. Comin, M. Yuan, E. Alarousu, A. Buin, Y. Chen, S. Hoogland, A. Rothenberger, K. Katsiev, Y. Losovyj, X. Zhang, P. A. Dowben, O. F. Mohammed, E. H. Sargent, O. M. Bakr, *Science* **2015**, 347, 519.
- [48] Q. Nian, D. Look, K. Leedy, G. J. Cheng, *Appl. Phys. A* **2018**, 124, 633.
- [49] J. Xing, X. Zheng, Z. Yu, Y. H. Lei, L. Hou, Y. T. Zou, C. Zhao, B. Wang, H. T. Yu, D. X. Pan, Y. C. Zhai, J. L. Cheng, D. Zhou, S. N. Qu, J. J. Yang, R. A. Ganeev, W. L. Yu, C. L. Guo, *Adv. Opt. Mater.* **2018**, 6, 1800411.